International Journal of Thermophysics, Vol. 25, No. 6, November 2004 (© 2004)

Lennard-Jones Viscosities in Wide Ranges of Temperature and Density: Fast Calculations Using a Steady–State Periodic Perturbation Method

V. R. Vasquez,[1,2] E. A. Macedo,[3] and M. S. Zabaloy[4]

Received December 24, 2003

A method for fast calculation of viscosity from molecular dynamics simulation is revisited. The method consists of using a steady-state periodic perturbation. A methodology to choose the amplitude of the external perturbation, which is one of the major practical issues in the original technique of Gosling et al. [Mol. Phys. **26**: 1475 (1973)] is proposed. The amplitude of the perturbation required for fast caculations and the viscosity values for wide ranges of temperature and density of the Lennard-Jones (LJ) model fluid are reported. The viscosity results are in agreement with recent LJ viscosity calculations. Additionally, the simulations demonstrate that the proposed approach is suitable to efficiently generate viscosity data of good quality.

KEY WORDS: Lennard-Jones; molecular dynamics; periodic perturbation methods; transport properties; viscosity.

1. INTRODUCTION

Rheological properties of hydrocarbons and other substances, viscosity in particular, over wide ranges of temperature and pressure are used, e.g., in petroleum reservoir simulation and in high pressure lubrication applications. Computational fluid dynamics (CFD) codes, which are used to solve

[1]Chemical Engineering Department, University of Nevada, Reno, Reno, Nevada 89557, U.S.A.

[2]To whom correspondence should be addressed. E-mail: vvasquez@unr.edu.

[3]Laboratory of Separation and Reaction Engineering, Departamento de Enghenharia Química, Faculdade de Engenharia da Universidade do Porto, Rua Dr. Roberto Frias s/n, 4200-465 Porto, Portugal.

[4]Planta Piloto de Ingeniería Química, PLAPIQUI (UNS-CONICET), Camino La Carrindanga Km 7, Casilla de Correo 717, 8000 Bahia Blanca, Argentina.

0195-928X/04/1100-1799/0 © 2004 Springer Science+Business Media, Inc.

the conservation equations in problems where heat, mass and momentum transport occur simultaneously, rely on models for estimating the fluid viscosities, among other physical properties [1]. Correlations for heat and mass transfer coefficients also use fluid viscosities as input [2]. Analytical models for viscosity as a function of temperature, pressure and composition, able to interpolate and extrapolate known experimental information, are required to fulfill the need of having to compute reliable viscosity values. Monnery et al. [3] reviewed the practical predictive and correlative methods for viscosity. They concluded that the most promising new viscosity modeling approaches appeared to be those based on statistical mechanics. Models based on statistical mechanics are those that specify an intermolecular potential function. Zabaloy et al. [4] assessed the potential of using a modeling approach for viscosity based on the properties of the Lennard-Jones (LJ) model fluid, computed through molecular simulation. Zabaloy et al. [4] also described possible ways in which molecular simulation data can be used, and showed that, despite the simplicity of the LJ intermolecular potential function, it describes the same basic trends found for the viscosity of real fluids in wide ranges of temperature and pressure. Through the use of effective values for the intermolecular potential parameters, even the behavior of relatively complex fluids can be represented by the LJ fluid [4].

Several molecular simulation methods can be found in the literature to calculate viscosity and other transport properties. These are mainly categorized as equilibrium and nonequilibrium methods. In the equilibrium methods, the viscosity is obtained from momemtum or pressure fluctuations [5,6] using Green–Kubo relationships. In nonequilibrium methods, the viscosity is computed from the response of applying a steady-state shear [6]. Equilibrium methods are computationally expensive, and for fast estimates of transport properties, they are usually not practical. On the other hand, nonequilibrium methods are more convenient. Among these, the SLLOD algorithm [7] (its name is in association with the DOLLS algorithm of Evans and Morris [7]) is very popular. Here, the viscosity is obtained by imposing a Couette flow, with modified equations of motion and using sliding boundary conditions [7]. In the SLLOD algorithm, the viscosity has to be calculated as a function of the shear rate and then extrapolated to zero shear to obtain the Newtonian viscosity. The viscosity calculations at low shear rate can be computationally time consuming and the implementation of the method is not necessarily straightforward. Another possibility is to apply a known external potential such that the response of the system is analytically linked to the Newtonian viscosity. The magnitude and form of the external potential is chosen such that its effects are easy to measure. Gosling et al. [8] proposed a method where a

simple acceleration, in a given direction, is set on every particle. Then the viscosity is obtained from the developed drift–velocity profile. Gosling's method [8] turns out to be very efficient computationally.

In this work, we explore in detail the use of Gosling's approach for calculating viscosities of the LJ fluid (see details of the method in Section 2). We find that the approach is very efficient computationally when appropriate values of the magnitude of the external potential are used. We propose a methodology to choose the amplitude of the external force and suggest a series of these values in ranges of temperature and density wider than in the available literature. The main advantage of Gosling's approach is that its implementation is straightforward and it can be incorporated with ease within any standard molecular dynamics code. The results of this work can be used as a guideline to choose the value of the amplitude of the external force to quickly obtain viscosity values for model fluids. The purpose of the present work is to evaluate the performance of Gosling's approach with regard to speed and quality of the computed viscosity, for wide temperature and density ranges. We anticipate the use of a similar approach for LJ mixtures. To our knowledge, viscosity data for LJ mixtures are available only at a limited number of conditions (e.g., Murad [9]). On the other hand, Meier [10,20] has recently produced high quality viscosity data for the pure LJ fluid through equilibrium molecular dynamics.

In Section 2, we discuss Gosling's approach including implementation details. Section 3 describes the approach we propose for the calculation of the amplitude of the external force. Section 4 discusses the details of the simulation model used in this work. Section 5 contains the results and a brief discussion of the main findings. Finally, Section 6 gives some concluding remarks and suggestions for future work.

2. STEADY–STATE PERIODIC PERTURBATION METHOD

As mentioned in the introduction, many of the methods used in molecular simulation to estimate transport properties require significant computational time to obtain good statistics in the calculations. A way to accelerate the calculation of these transport coefficients, viscosity in particular, is to monitor the response of the system to a known external potential field. Our description of the external field method used in this work follows closely that of Gosling et al. [8]. LJ particles in the NVT ensemble are subject to an external potential field such that a force $\mathbf{F}(\mathbf{r}, t)$ is imposed on each particle at coordinates $\mathbf{r}$ and time t. The hydrodynamics

of the system is described by the Navier–Stokes equation [11]

$$\rho\frac{\partial \mathbf{u}}{\partial t}+\rho(\mathbf{u}\cdot\nabla)\mathbf{u}=(\rho/m)\mathbf{F}(\mathbf{r},t)-\nabla P+\eta\nabla^2\mathbf{u}, \tag{1}$$

where P is the pressure, $\mathbf{u}$ is the fluid velocity field representing the number average of the molecular velocities at the *point* for which the Navier–Stokes equation is written, m is the mass of an individual particle, ρ is the mass density, and η is the shear viscosity. Equation (1) is a continuum mechanics equation. It comes from combining the differential equations of continuity and motion for the Newtonian fluid case [2]. The forces that must appear within the Navier–Stokes equation are those acting on the continuum system i.e., forces exerted by the fluid surrounding the system and body forces such as gravity or any other external field. Since the concept of molecule is not defined in terms of a continuum picture [12], contributions from intermolecular forces do not appear explicitly in the Navier–Stokes equation.

The main idea of the method is to choose an external force or potential such that the analytical solution of the Navier–Stokes equation is relatively easy to obtain. Such solution should link the developed velocity field with the shear viscosity. The developed velocity field comes in turn as the result of averaging molecular velocities obtained from a molecular dynamics run. Additionally, the external force has to be consistent with the periodic boundary conditions used in the simulation box. The choice made by Gosling et al. [8] consists of a force $\mathbf{F}(\mathbf{r},t)$ directed along the x direction with a magnitude varying with z and independent of x, y and time. Additionally, the component x of the force is zero at the cell boundaries in the z direction. With these conditions for the external force and with no pressure gradient in the x-direction, Eq. (1) becomes

$$\rho\frac{\partial u_x(z,t)}{\partial t}=(\rho/m)F_x(z)+\eta\frac{\partial^2 u_x(z,t)}{\partial z^2}. \tag{2}$$

A common choice for $F_x(z)$ in Eq. (2) are periodic functions such as

$$F_x(z)=m\gamma\ \sin(2\pi nz/L_z), \tag{3}$$

where $z=0$ and $z=L_z$ represent the boundaries of the simulation box, n is a dimensionless integer greater than zero, and γ is a constant, having units of acceleration, proportional to the amplitude. $F_x(z)$ has to be zero at the cell boundaries in order to satisfy the periodic conditions.

Equation (2) can now be solved at steady-state conditions to give the velocity profile

$$u_x(z)=(\rho L_z^2\gamma/4\pi^2n^2\eta)\sin(2\pi nz/L_z), \tag{4}$$

where the boundary conditions $u_x(0) = 0$ and $u_x(L_z) = 0$ are imposed. The above solution was obtained assuming that the fluid density and fluid viscosity are both constant. For a pure Newtonian fluid this is strictly true if two variables such as pressure and temperature are held constant, i.e., independent from position at steady state. From Eq. (4), the resulting steady-state velocity profile is also sinusoidal, in phase with $F_x(z)$, and the amplitude is directly proportional to γ and inversely proportional to η. From Eq. (4) one can see that there is a direct relation between the velocity and the viscosity η. Therefore, in principle, all that one has to do is to characterize the drift velocity profile to obtain the shear viscosity. More specifically, the viscosity η is computed by curve fitting (using Eq. (4)) the fluid velocity profile obtained from a molecular dynamics run. For convenience, Eq. (4) is re-arranged further as

$$u_x(z) = u_0 \sin(2\pi n z/L_z) \tag{5}$$

from which the viscosity η is given by

$$\eta = \frac{\rho L_z^2 \gamma}{4\pi^2 n^2 u_0}. \tag{6}$$

2.1. General Implementation Issues

Although the implementation of this method is fairly simple, there are some difficulties that have to be analyzed carefully. The first is that Eq. (5) is only valid in the limit $k \to 0$, where

$$k = 2\pi n/L_z. \tag{7}$$

In other words, it is valid only in the long wave limit [8]. The reason is that the Navier–Stokes equation is applicable only to a continuum, and hence the wavelength of the external field has to be large in comparison to the molecular dimensions. By looking at the definition of k, there are only two ways to aproximate this: (a) choosing the smallest value n, which is one, and (b) using large values of L_z, which is constrained by the computational cost. For this work, the approach used is discussed in Section 4. Hess [6], in a comparison of different methods for computing the shear viscosity of model liquids, discusses the issue of the dependence of the viscosity with k for a perturbation method similar to the present one. His findings indicate that at $n = 1$ this dependency is small, but measurable.

The other issue is how to choose the input value of γ required by the MD code to compute the fluid velocity field. There is no rigorous solution to this problem reported in the literature. γ has to be large enough

to produce a well-defined drift velocity profile, but if it is too large it can cause significant temperature drift in the system and it can produce shear rates beyond the Newtonian range which would invalidate Eq. (4). In other words, large values of γ can impact the model fluid in such a way that the system is no longer representative of the original conditions, e.g., low enough shear rate, at which one wants to measure the viscosity η. Gosling et al. [8] suggests estimating γ by using a force of one-tenth of the root-mean-square force that arises from the MD simulation. On the other hand, Hess [6] proposes not exceeding the maximum shear rate

$$s_{\max} = \max_z \left| \frac{\partial u_x(z)}{\partial z} \right| = \gamma \frac{\rho}{\eta k} \tag{8}$$

to avoid the system moving too far from equilibrium. The value of $s_{\max}$ (required to compute γ from Eq. (8)) is estimated somewhat empirically. For instance, one can use the temperature drift as a measure of how far the system is from equilibrium and then use this as a tradeoff to estimate $s_{\max}$. The other possibility is to use known values of viscosity [6].

Once a decision is made about k and γ, the use of the method consists of adding an acceleration to each particle in the MD simulation according to Eq. (3). Then, one has to allow a reasonable simulation time for the drift-velocity profile to develop to steady-state conditions. The unsteady-state solution of Eq. (2) is of the form [6]

$$u_x(z) = (\rho L_z^2 \gamma / 4\pi^2 n^2 \eta)(1 - e^{-t/\tau_r})) \sin(2\pi n z / L_z), \tag{9}$$

where

$$\tau_r = \frac{\rho L_z^2}{4\eta\pi^2 n^2}. \tag{10}$$

From Eq. (9), one sees that t has to be large enough for the term e^{-t/τ_r} to be small. According to Hess [6], a value of $t = 5\tau_r$ should be reasonable for most purposes. Once the drift-velocity profile has developed, the z-side of the simulation box (L_z) is divided into intervals or bins, where information about the x-component of the particles velocity is recorded and averaged. The computed averages are set to correspond to z-coordinates at the midpoint of the bin. Then the drift velocity is fitted to Eq. (5) using the method of least squares. The viscosity is calculated using Eq. (6) with the value u_0 obtained from the least squares regression. Statistics about the viscosity are collected throughout the simulation. In other words, the velocity profile is fitted throughout the simulation and then the viscosity is calculated such that statistical information about the variation observed is recorded. One can monitor this variation and estimate when there is

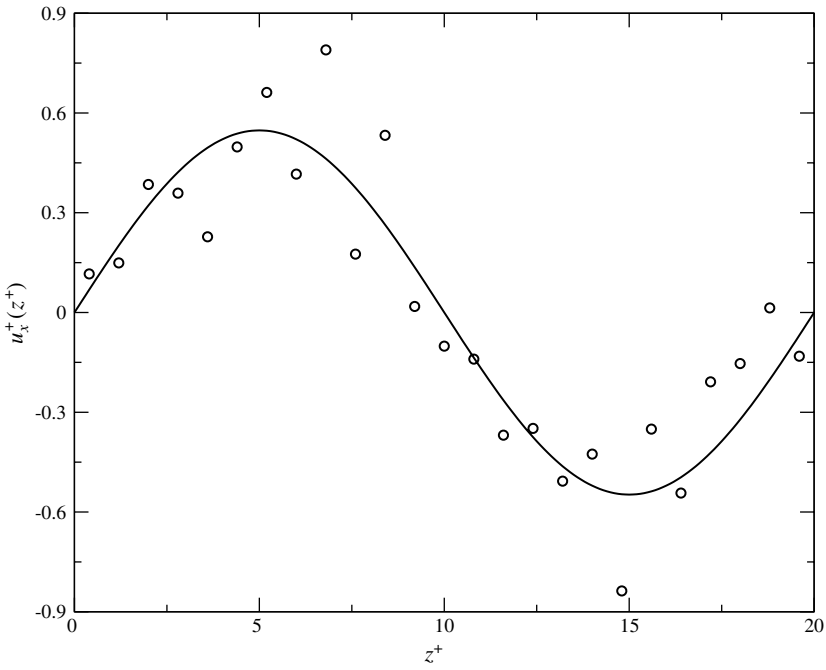

Fig. 1. Typical steady-state drift–velocity profile observed during the simulations for viscosity calculations (circles). The solid line corresponds to Eq. (5) after determining u_0 by least–squares minimization. The velocity profile corresponds to the simulation conditions $T^+ = 1.3$, $\rho^+ = 0.5$, and $\gamma^+ = 0.07783$. The average viscosity associated with the predicted velocity profile (solid line) is $\langle \eta^+ \rangle = 0.72$.

no further improvement in the precision of the calculations. At that point one could stop the simulation or a try different value of γ^+. Figure 1 shows a typical drift–velocity profile obtained from MD simulation (circles) and the predicted velocity profile by Eq. (5), with u_0 obtained from least-squares regression (solid line).

3. PROPOSED SCHEME FOR THE ESTIMATION OF γ

The methods to estimate γ proposed by Gosling et al. [8] and Hess [6] work well within the conditions of their simulations. We notice that for wider ranges of temperature and density, those recipes do not work well. In some cases, unstable drift velocity profiles develop and in others the computed viscosity presents a significant shift with respect to previously reported results. The method we propose here consists simply

of the following steps: (a) set the temperature T and ρ conditions at which the viscosity value needs to be computed, (b) perform a series of MD simulations at the set T and ρ values, in a wide enough range of values of γ, (c) plot the computed viscosity as a function of γ, and (d) read the value of viscosity and the value of γ from the region in the plot where η is a fairly constant and stable function of γ. Figure 2 shows an example of such a plot. At low values of γ, the computed viscosity values are scattered. This is because the external force is too weak to develop a stable drift–velocity profile. A stable region is observed where the viscosity value does not change significantly with changes in the value of γ. This second region is the one that should be used to arrive at a value of viscosity and to choose an appropriate range of values for the amplitude of the force, i.e., for γ. If, as we did in this work, the viscosity is directly read at some γ value within this second region, then, the read viscosity

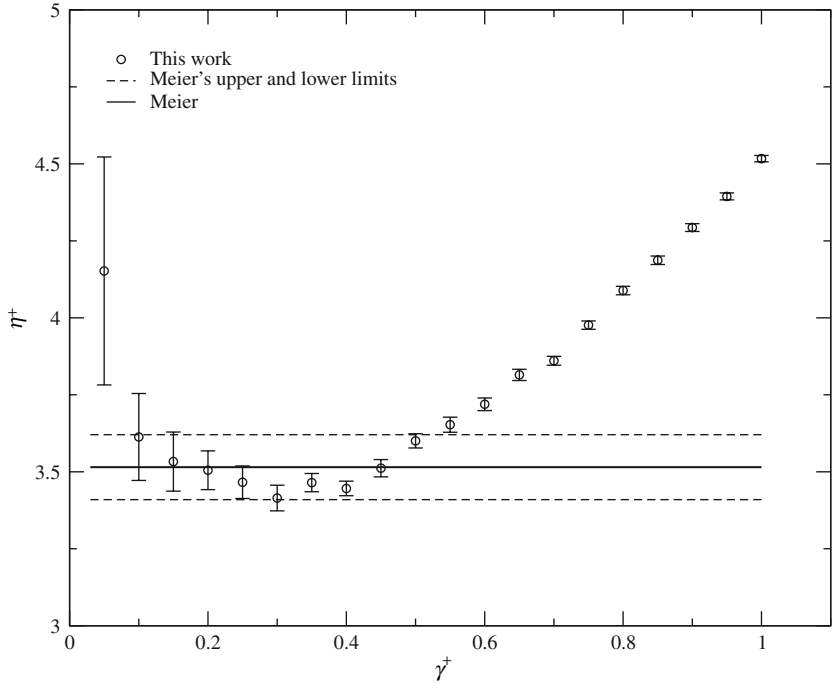

Fig. 2. Viscosity η^+ (Eq. (17)) as a function of the external amplitude γ^+ (Eq. (16)) for the LJ fluid at $T^+ = 0.7$ (Eq. (13)) and $\rho^+ = 0.85$ (Eq. (15)). The central solid horizontal line corresponds to the viscosity reported by Meier et al. [10, 20] using equilibrium molecular dynamics methods. The dashed lines correspond to the upper and lower uncertainty limits of Meier's calculations.

should be regarded as a first approximation to the Newtonian viscosity. The second region is also the region of choice to read a set of viscosity values to be extrapolated to zero shear rate if a viscosity value in principle closer to the Newtonian limit is desired. Finally, in the third region, the value of viscosity becomes a noticeable function of the amplitude factor γ. In this case, the external force is strong enough to cause the system to move away from equilibrium significantly. In other words, the internal stresses are strong enough to move the system into the non-Newtonian regime, within which our basic working equation, Eq. (5), for computing the viscosity is no longer valid.

4. SIMULATION MODEL

To test Gosling's approach in wide ranges of temperature and density, we use the LJ intermolecular potential,

$$\phi(r) = 4\epsilon\left[\left(\frac{\sigma}{r}\right)^{12} - \left(\frac{\sigma}{r}\right)^{6}\right], \tag{11}$$

where $\phi(r)$ is the potential energy at separation distance r, ϵ is the LJ well depth and σ is the separation distance at zero potential energy.

The fluid is modeled as a set of spherical molecules that interact with the cut and shifted LJ potential:

$$\phi_{cs}(r) = \begin{cases} \phi(r) - \phi(r_c) & \text{for } r < r_c, \\ 0 & \text{for } r > r_c, \end{cases} \tag{12}$$

where r_c is the cutoff radius of the potential.

The parameters and results of the simulations are specified using the reduced units

$$T^+ = \frac{k_B T}{\epsilon}, \tag{13}$$

$$P^+ = \frac{P\sigma^3}{\epsilon}, \tag{14}$$

$$\rho^+ = \frac{N}{V}\sigma^3, \tag{15}$$

$$\gamma^+ = \gamma\frac{m\sigma}{\epsilon}, \tag{16}$$

$$\eta^+ = \eta\frac{\sigma^2}{\sqrt{m\epsilon}}, \tag{17}$$

$$t^+ = (\epsilon/m\sigma^2)^{1/2}t, \tag{18}$$

$$z^+ = \frac{z}{\sigma}, \tag{19}$$

$$u_x^+ = u_x \sqrt{\frac{m}{\epsilon}}, \tag{20}$$

where k_B is the Boltzmann constant, T is the temperature, and V is the total volume.

All the simulations are performed in the NVT ensemble with $N = 1000$ LJ particles. The LJ potential cutoff radious is 5.0σ. A rectangular simulation box of dimensions $L_x = (N/2\rho_N)^{1/3}$, $L_y = L_x$, and $L_z = 2L_x$ is used, where ρ_N is the number density. The velocity Verlet algorithm [13–15] is used for the integration of the equations of motion with a dimensionless time step of $\delta t^+ = 0.005$ and using standard periodic boundary conditions [13]. The absolute temperature is controlled with the Nosé–Hoover thermostat [13,14,16,17] using a coupling constant of $Q = 10.0$.

5. RESULTS AND DISCUSSION

The distribution of the simulated state points in the T^+-ρ^+ plane is presented in Fig. 3. There are two types of points in this figure: the circles indicate points where the value of γ^+ is estimated using the procedure described in Section 3, and the stars are points where γ^+ is estimated by interpolating the information represented by the circles. Figure 3 shows that we covered all possible fluid states (liquid, vapor, high and low density supercritical fluid).

Before calculating the viscosities, we validated our LJ MD code, without the influence of any external field, by comparing the calculated PVT behavior against the values computed from the accurate Kolafa–Nezbeda LJ equation of state [18]. The working PVT equations of the Kolafa–Nezbeda equation of state are summarized concisely by Zabaloy et al. [4]. Figure 4 shows some of the validation results, and we can see that the agreement is excellent. Long range corrections were used in the pressure calculations according to [19]

$$P_{lrc}^+ = \frac{32}{9}\pi(\rho^+)^2 \left[\left(\frac{\sigma}{r_c}\right)^9 - \frac{3}{2}\left(\frac{\sigma}{r_c}\right)^3 \right], \tag{21}$$

where P_{lrc}^+ is the correction term added to the P^+ value computed by the MD code. Figure 2 shows a typical plot of the η^+ versus γ^+. Here we can see the three regions described in Section 3. As Figs. 5 and 6 illustrate, not all of the plots are alike. In some, the third region is not as pronounced, and in others, the second region is better defined. Usually, preliminary

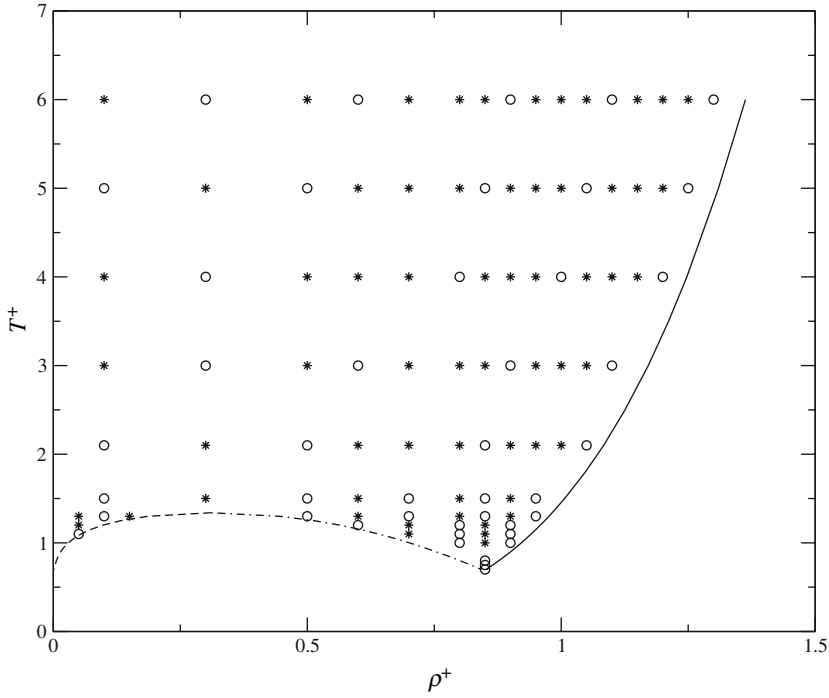

Fig. 3. Distribution of the simulated state points in the T^+–ρ^+ plane. The circles are the points where the value of γ^+ is obtained according to the methodology of Section 3 and the stars are the points where γ^+ is obtained by interpolation using the circle points. The solid line represents the LJ fluid density–temperature locus at solid–fluid equilibrium and the dashed–line the LJ saturated fluid vapor–liquid equilibrium locus (see Ref. [4] for details).

runs have to be performed to determine an appropriate range for γ^+, and then refined runs are performed for final estimation of γ^+ and η^+. The number of required preliminary runs increases with the user's desired level of accuracy in the identification of the stable noise-free region.

Figure 7 presents a typical plot of the calculated viscosity as a function of the simulation time. We can see that the average value of viscosity in the simulation stabilizes fairly quickly. Figure 7 also shows that the temperature is properly controlled by the chosen thermostat. For most of the points in the T^+-ρ^+ plane, the calculations are fast, but the computational cost increases with the density. In general, the computational time required when using equilibrium methods varies between 1.5 and 2.0 million steps in the production phase [5,10,20], which is far larger than the time required using the method described in this work. This is true even if

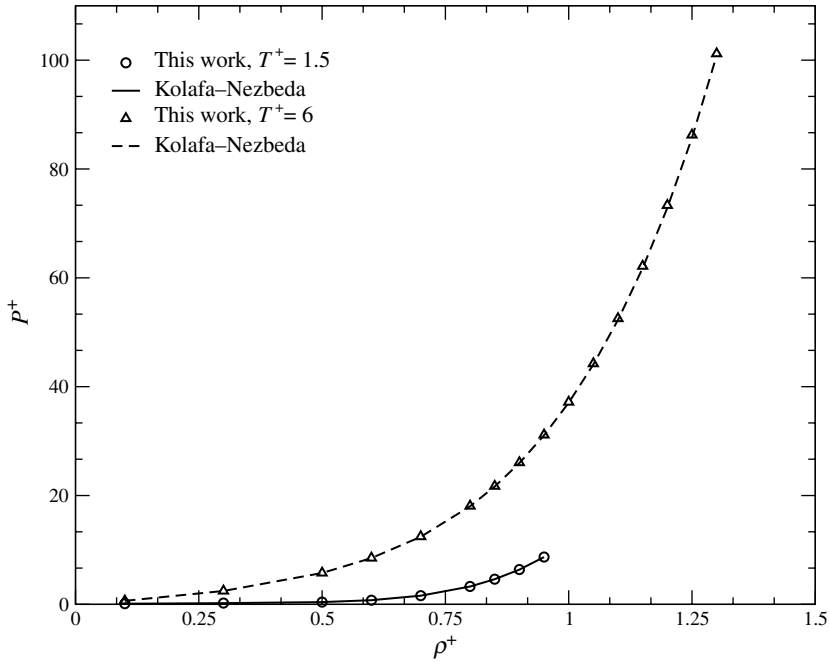

Fig. 4. Comparison of the PTρ behavior of the LJ fluid for the simulated state points. The lines correspond to the Kolafa–Nezbeda LJ equation of state [18] and the simulated results are represented by triangles up and circles.

one has to carry out a number of runs to determine an appropriate value of γ^+ (thus following the methodology of Section 3).

The viscosity results obtained for the LJ fluid and the values of γ^+ suggested for the conditions of Fig. 3 are presented in Table I. Additionally, information about the statistical uncertainty associated with the calculations is presented for T^+ and η^+. We also show in Table I the viscosity value computed by Meier et al. [10,20] and the relative difference between the viscosity computed here and the Meier et al. [10,20] result, when available. The ranges we suggest for γ^+ arise from visual observation of plots such as Figs. 2, 5, 6. They do not represent optimal ranges. Therefore a deeper analysis, such as that of Ref. [21], would be required to refine further the viscosity calculations and their uncertainty estimates. To fix ideas, the first line in Table I shows that in a single run, using as input $\rho^+ = 0.05$, $T^+ = 1.300$, and an external field of $\gamma^+ = 0.079883$, we estimate an average viscosity of $\eta^+ = 0.1420$ with an error bar of $\sigma_{\eta^+} = \pm 0.0008$. The error bar of the measured temperature for this case is $\sigma_{T^+} = \pm 0.006$.

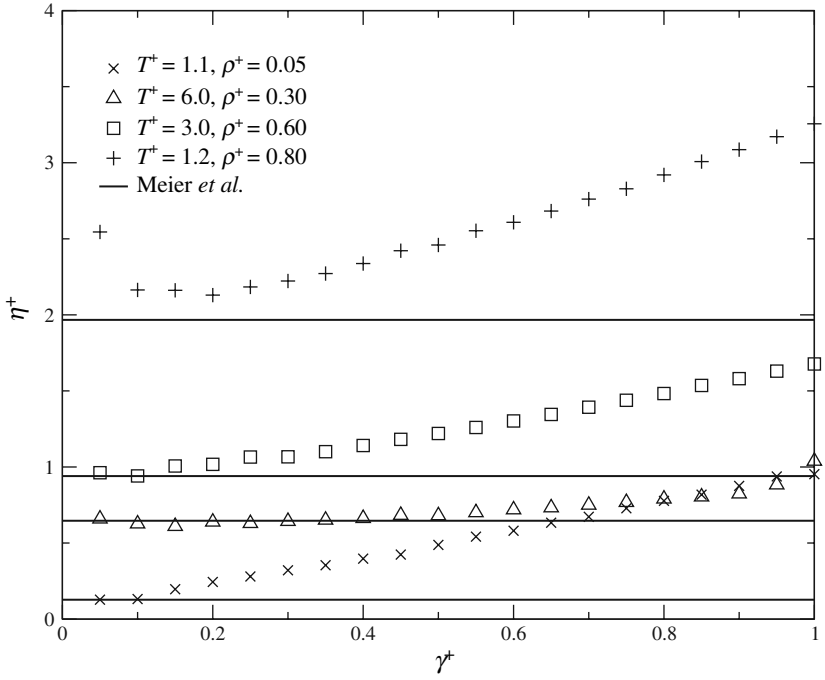

Fig. 5. Illustration of how the shape of the viscosity versus external field amplitude curve varies with the temperature and the density (see conditions in the graph). The error bars have been removed to avoid overloading the figure.

The number $\pm\Delta\gamma^+ = 0.028467$ means that we expect to obtain accurate values of the viscosity within the range $\gamma^+ = 0.079883 \pm 0.028467$. The first line in Table I also shows that the value Meier et al. [10,20] computed is $\eta_M^+ = 0.1499$. Our value is hence around 5% less than Meier et al. [10,20] value. Hence $D\% = -5$. The number $D\%$ is formally defined as the percent difference between our result and Meier et al. [10,20] result at the same conditions. The reported σ_{η^+} values are statistical uncertainties in viscosity and reflect the variability for the computed viscosity at the set value of γ^+. The values of the average viscosity reported in Table I are a direct output of the simulations. In other words, no extrapolating scheme at zero shear rate is used. Such schemes are still a matter of considerable debate [21]. The values of the average viscosity reported in Table I do not correspond either to averaging η^+ values computed at a number of γ^+ values within the accepted γ^+ range. The availability of Meier et al. [10,20] accurate viscosity data, which, we regard here as standard reference data, allowed us to make fast independent estimates of

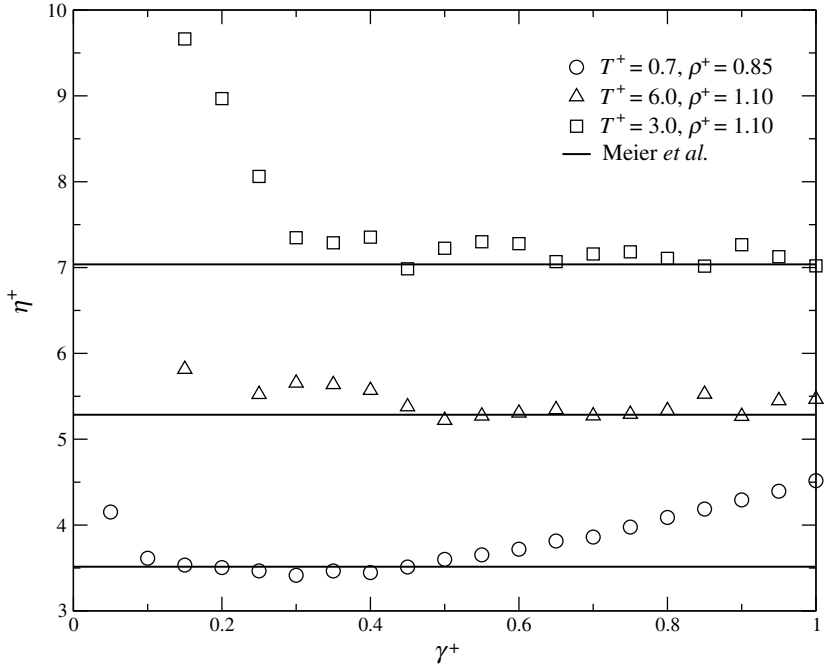

Fig. 6. Illustration of how the shape of the viscosity versus external field amplitude curve varies with the temperature and the density (see conditions in the graph). The error bars have been removed to avoid overloading the figure.

the overall uncertainty of our calculated viscosities by direct comparison with Meier et al. [10,20] results, as shown in the last column of Table I. When no standard reference data are available, the user should, for every studied thermodynamic state, carry out a careful analysis of the type of the one described by Yang et al. [21] and, if possible, compare at least some of the results with those obtained using a different molecular simulation technique. A detailed analysis of results as in Ref. [21] is beyond our goals in the present exploratory work. Such an analysis, if carried out, should reduce the discrepancies reported in Table I, between our and Meier et al. [10,20] data.

Figure 8 shows a comparison of viscosity values obtained from this work with the standard reference data of Meier [10,20]. We can observe that, in general, the agreement is very reasonable, which suggests that the approach discussed in this work is a good alternative for fast viscosity calculations of model fluids such as LJ.

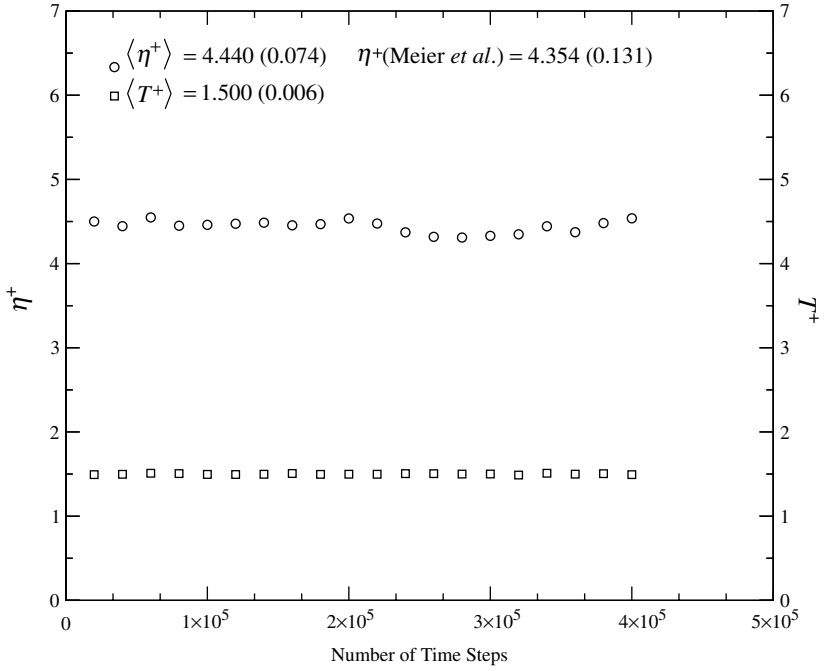

Fig. 7. Viscosity and temperature as a function of the simulation time (number of time steps) for the LJ fluid at $T^+ = 1.5$, $\rho^+ = 0.95$, and $\gamma^+ = 0.45$. Notice that the average for both viscosity and temperature stabilizes early on in the simulation.

6. CONCLUSIONS

We show that reliable LJ viscosities, in wide ranges of temperature and density, can be obtained relatively quickly from MD simulations using a modified steady-state periodic perturbation method introduced by Gosling et al. [8]. Additionally, we propose a methodology to choose the amplitude of the perturbation, which is one of the major practical problems in the original technique of Gosling et al. [8]. For the LJ fluid, we report both amplitude and viscosity values for wide ranges of temperature and density. The results show satisfactory agreement with recent LJ viscosity calculations obtained using more traditional approaches based on equilibrium pressure fluctuations and the Green–Kubo formula or Einstein methods. The simulation results demonstrate that the approach proposed is suitable to generate viscosity data of enough quality to support, for instance, the development of semi–empirical models for real fluids with a stronger fundamental basis. Additionally, the method is very efficient

Table I. Simulation Results for η^+ of the LJ Model Fluid

ρ^+	T^+	σ_{T^+}	η^+	σ_{η^+}	γ^+	$\pm\Delta\gamma^+$	η_M^+	D (%)
0.05	1.300	0.006	0.1420	0.0008	0.079883	0.028467	0.14990	−5
0.05	1.200	0.006	0.1364	0.0005	0.079883	0.028467	0.14180	−4
0.05	1.100	0.005	0.1318	0.0006	0.079883	0.028467	0.12760	3
0.10	6.000	0.036	0.4354	0.0226	0.079881	0.028470	0.51080	−15
0.10	5.000	0.030	0.4410	0.0247	0.079881	0.028470	N/A	N/A
0.10	4.000	0.024	0.3696	0.0095	0.079881	0.028470	0.40370	−8
0.10	3.000	0.018	0.2994	0.0082	0.079881	0.028470	0.32430	−8
0.10	2.100	0.012	0.2378	0.0042	0.079881	0.028470	0.25670	−7
0.10	1.500	0.008	0.2043	0.0019	0.079881	0.028470	0.19890	3
0.10	1.300	0.007	0.1946	0.0012	0.079881	0.028470	0.16860	15
0.15	1.300	0.006	0.2309	0.0016	0.079863	0.028484	0.18040	28
0.30	6.000	0.033	0.6166	0.0264	0.079416	0.028840	0.64650	−5
0.30	5.000	0.029	0.5861	0.0266	0.079416	0.028840	N/A	N/A
0.30	4.000	0.023	0.5126	0.0168	0.079416	0.028840	0.50140	2
0.30	3.000	0.017	0.4668	0.0100	0.079416	0.028840	0.43480	7
0.30	2.100	0.012	0.4046	0.0087	0.079416	0.028840	0.37830	7
0.30	1.500	0.008	0.3693	0.0034	0.079416	0.028840	0.32750	13
0.50	6.002	0.035	0.9131	0.0457	0.077827	0.031140	0.92720	−2
0.50	5.001	0.028	0.9582	0.0794	0.077827	0.031140	N/A	N/A
0.50	4.000	0.023	0.8072	0.0287	0.077827	0.031140	0.77350	4
0.50	3.000	0.016	0.7390	0.0139	0.077827	0.031140	0.72030	3
0.50	2.100	0.012	0.7578	0.0145	0.077827	0.031140	0.62510	21
0.50	1.500	0.008	0.6975	0.0123	0.077827	0.031140	0.58180	20
0.50	1.300	0.007	0.7392	0.0111	0.077827	0.031140	0.55450	33
0.60	6.001	0.036	1.2965	0.0875	0.080668	0.033461	1.14600	13
0.60	5.000	0.029	1.1403	0.0692	0.080668	0.033461	N/A	N/A
0.60	4.000	0.023	1.0296	0.0562	0.080668	0.033461	0.99280	4
0.60	3.000	0.017	0.9736	0.0385	0.080668	0.033461	0.94010	4
0.60	2.100	0.012	0.9272	0.0212	0.080668	0.033461	0.88740	4
0.60	1.500	0.008	0.9325	0.0242	0.080668	0.033461	0.84190	11
0.60	1.300	0.007	0.9370	0.0226	0.080668	0.033461	0.82820	13
0.60	1.200	0.007	0.9531	0.0190	0.080668	0.033461	0.80700	18
0.70	6.000	0.034	1.8731	0.2128	0.095753	0.037095	1.45800	28
0.70	5.000	0.030	1.6263	0.1280	0.095753	0.037095	N/A	N/A
0.70	4.000	0.023	1.3389	0.0461	0.095753	0.037095	1.35300	−1
0.70	3.000	0.017	1.3519	0.0487	0.095753	0.037095	1.30700	3
0.70	2.100	0.012	1.2713	0.0327	0.095753	0.037095	1.26100	1
0.70	1.500	0.009	1.2505	0.0240	0.095753	0.037095	1.18900	5
0.70	1.300	0.007	1.3185	0.0315	0.095753	0.037095	1.22300	8
0.70	1.200	0.007	1.3251	0.0253	0.095753	0.037095	1.19000	11
0.70	1.100	0.006	1.3111	0.0240	0.095753	0.037095	1.20100	9
0.80	6.001	0.033	2.1213	0.1125	0.141221	0.043831	1.94000	9
0.80	4.999	0.029	2.1025	0.1506	0.141221	0.043831	N/A	N/A
0.80	4.000	0.023	1.8157	0.0573	0.141221	0.043831	1.84900	−2
0.80	3.000	0.017	1.8378	0.0655	0.141221	0.043831	1.83200	0

Table I. (*Continued*)

ρ^+	T^+	σ_{T+}	η^+	σ_{η^+}	γ^+	$\pm\Delta\gamma^+$	η_M^+	D (%)
0.80	2.100	0.012	1.9821	0.0503	0.141221	0.043831	1.86300	6
0.80	1.500	0.008	1.9274	0.0475	0.141221	0.043831	1.91200	1
0.80	1.300	0.008	2.1221	0.0490	0.141221	0.043831	1.97100	8
0.80	1.200	0.007	2.1256	0.0374	0.141221	0.043831	1.96700	8
0.80	1.100	0.006	2.0538	0.0374	0.141221	0.043831	2.01900	2
0.80	1.000	0.006	2.1310	0.0445	0.141221	0.043831	2.05300	4
0.85	6.000	0.035	2.3221	0.1024	0.184924	0.049688	2.23900	4
0.85	5.001	0.028	2.2054	0.0643	0.184924	0.049688	N/A	N/A
0.85	4.000	0.023	2.2726	0.0759	0.184924	0.049688	2.15600	5
0.85	3.000	0.017	2.2837	0.0660	0.184924	0.049688	2.25800	1
0.85	2.100	0.012	2.4819	0.0685	0.184924	0.049688	2.31500	7
0.85	1.500	0.009	2.6863	0.0695	0.184924	0.049688	2.43900	10
0.85	1.300	0.007	2.7526	0.0661	0.184924	0.049688	2.52900	9
0.85	1.200	0.007	2.7598	0.0617	0.184924	0.049688	2.65800	4
0.85	1.100	0.006	2.9004	0.0670	0.184924	0.049688	2.62300	11
0.85	1.000	0.006	3.0157	0.0680	0.184924	0.049688	2.83300	6
0.85	0.800	0.004	3.3257	0.0674	0.184924	0.049688	3.24600	2
0.85	0.750	0.004	3.3150	0.0682	0.184924	0.049688	N/A	N/A
0.85	0.700	0.004	3.4909	0.0726	0.184924	0.049688	3.51500	−1
0.90	5.998	0.034	2.6838	0.0941	0.250175	0.058508	2.65400	1
0.90	5.001	0.028	2.5971	0.0681	0.250175	0.058508	N/A	N/A
0.90	4.000	0.023	2.7607	0.0717	0.250175	0.058508	2.65900	4
0.90	3.000	0.017	2.7906	0.0736	0.250175	0.058508	2.75100	1
0.90	2.100	0.012	3.1435	0.0652	0.250175	0.058508	2.94200	7
0.90	1.500	0.009	3.3071	0.0607	0.250175	0.058508	3.28700	1
0.90	1.300	0.007	3.5943	0.0790	0.250175	0.058508	3.53900	2
0.90	1.200	0.007	3.6930	0.0823	0.250175	0.058508	3.62700	2
0.90	1.100	0.006	3.8793	0.0759	0.250175	0.058508	3.81400	2
0.90	1.000	0.006	3.9771	0.0712	0.250175	0.058508	3.96900	0
0.95	6.000	0.035	3.1033	0.0650	0.344637	0.071824	3.15100	−2
0.95	5.000	0.029	3.2178	0.0916	0.344637	0.071824	N/A	N/A
0.95	4.000	0.022	3.3246	0.0875	0.344637	0.071824	3.26600	2
0.95	3.000	0.017	3.4760	0.0760	0.344637	0.071824	3.36900	3
0.95	2.100	0.012	3.8561	0.0751	0.344637	0.071824	3.74700	3
0.95	1.500	0.009	4.5366	0.1111	0.344637	0.071824	4.35400	4
0.95	1.300	0.007	4.8259	0.0899	0.344637	0.071824	4.89700	−1
1.00	6.001	0.034	3.7958	0.0990	0.477914	0.091768	3.62600	5
1.00	4.999	0.028	3.7927	0.0845	0.477914	0.091768	N/A	N/A
1.00	3.999	0.023	4.0959	0.0776	0.477914	0.091768	3.86600	6
1.00	3.000	0.017	4.3710	0.0791	0.477914	0.091768	4.25300	3
1.00	2.100	0.012	5.0321	0.0918	0.477914	0.091768	4.97200	1
1.05	5.999	0.034	4.4261	0.0898	0.661887	0.121224	4.47000	−1
1.05	4.999	0.029	4.6162	0.0786	0.661887	0.121224	N/A	N/A
1.05	4.000	0.023	5.0832	0.1097	0.661887	0.121224	4.69900	8
1.05	3.000	0.017	5.6246	0.1006	0.661887	0.121224	5.50000	2

Table I. (*Continued*)

ρ^+	T^+	σ_{T^+}	η^+	σ_{η^+}	γ^+	$\pm\Delta\gamma^+$	η_M^+	D (%)
1.05	2.100	0.012	6.5839	0.1071	0.661887	0.121224	N/A	N/A
1.10	6.002	0.034	5.3455	0.0876	0.911081	0.164014	5.28500	1
1.10	5.000	0.028	5.6708	0.0776	0.911081	0.164014	N/A	N/A
1.10	4.000	0.022	6.2673	0.0903	0.911081	0.164014	6.00800	4
1.10	3.001	0.017	7.1515	0.1036	0.911081	0.164014	7.03700	2
1.15	6.002	0.033	6.6647	0.0881	1.243073	0.225096	6.40200	4
1.15	5.000	0.028	7.0971	0.0709	1.243073	0.225096	N/A	N/A
1.15	4.000	0.023	7.8831	0.1033	1.243073	0.225096	7.81900	1
1.20	6.001	0.035	8.1744	0.1014	1.678934	0.310801	7.73000	6
1.20	4.998	0.028	8.8461	0.1017	1.678934	0.310801	N/A	N/A
1.20	4.000	0.022	9.9536	0.1264	1.678934	0.310801	N/A	N/A
1.25	6.000	0.033	9.9142	0.0873	2.243713	0.429095	9.75600	2
1.25	5.001	0.027	10.8679	0.1093	2.243713	0.429095	N/A	N/A
1.30	6.003	0.034	12.1865	0.1119	2.966961	0.589865	N/A	N/A

Suggested values of γ^+ and range are given for the conditions indicated of ρ^+ and T^+. These were obtained following the methodology of Section 3 without extrapolating to zero shear rate.

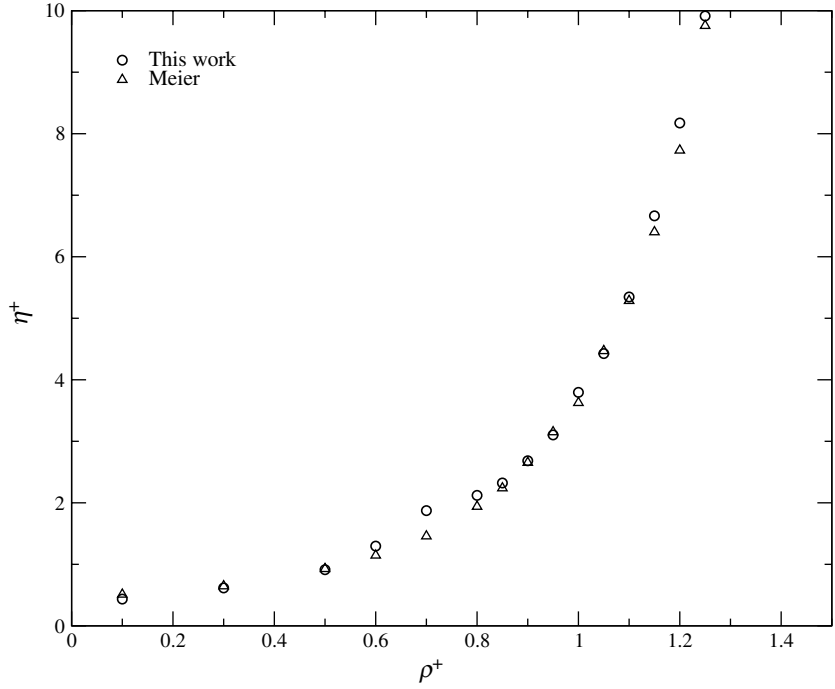

Fig. 8. Viscosity as a function of density for the LJ fluid at $T^+ = 6.0$. The results of this work (circles) are compared with the results reported by Meier et al. [10,20] (triangles).

computationally speaking when compared to equilibrium approaches. For example, there is no need for parallelization of the calculations and the results can be obtained reasonably fast with conventional computing facilities. To our knowledge, a fundamental study of the viscosity of mixtures of simple LJ fluids in wide enough ranges of composition, temperature and density, for pairs of LJ fluids with different enough values of the intermolecular potential parameters, is still lacking. We plan to address such a problem by extending the method described in this article to LJ mixtures.

ACKNOWLEDGMENTS

The authors would like to thank K. Meier, Institut für Thermodynamik, Universität der Bundeswehr Hamburg, Germany, for providing recent results on transport coefficients of the Lennard-Jones fluid, and to the Consejo Nacional de Investigaciones Científicas y Técnicas de la República Argentina for financial support to M. Zabaloy during his visit at University of Nevada, Reno.

REFERENCES

1. A. Bakker, A. Haidari, and L. Oshinowo, *Chem. Eng. Prog.* **97**:45 (2001).
2. C. Geankoplis, *Transport Processes and Separation Process Principles* (Prentice-Hall, Upper Saddle River, New Jersey, 2003).
3. W. D. Monnery, W. Y. Svrcek, and A. K. Mehrotra, *Can. J. Chem. Eng.* **73**:3 (1995).
4. M. S. Zabaloy, J. M. V. Machado, and E. A. Macedo. *Int. J. Thermophys.* **22**:829 (2001).
5. R. Rowley and M. Painter, *Int. J. Thermophys.* **18**:1109 (1997).
6. B. Hess, *J. Chem. Phys.* **116**:209 (2002).
7. D. Evans and G. Morris, *Statistical Mechanics of Nonequilibrium Liquids* (Academic Press, London, 1990).
8. E. Gosling, I. McDonald, and K. Singer, *Mol. Phys.* **26**:1475 (1973).
9. S. Murad, *AIChE J.* **32**:513 (1986).
10. K. Meier, *Computer Simulation and Interpretation of the Transport Coefficients of the Lennard-Jones Model Fluid* (Shaker Verlag, Aachen, 2002), ISBN 3-8322-0968-9.
11. R. Bird, W. Stewart, and E. Lightfoot, *Transport Phenomena* (John Wiley & Sons, New York, 1960).
12. J. Slattery, *Momentum, Energy and Mass Transfer in Continua* (McGraw Hill, New York, 1972).
13. M. Allen and D. Tildesley, *Computer Simulation of Liquids* (Oxford Science Publications, 1987).
14. D. Frenkel and B. Smit, *Understanding Molecular Simulation* (Academic Press, New York, 1996).
15. W. Swope, H. Andersen, P. Berens, and K. Wilson, *J. Chem. Phys.* **76**:637 (1982).
16. S. Nosé, *J. Chem. Phys.* **81**:511 (1984).
17. S. Nosé, *Mol. Phys.* **52**:255 (1984).

18. J. Kolafa and I. Nezbeda, *Fluid Phase Equilib.* **100**:1 (1994).
19. J. Johnson, J. Zollweg, and K. Gubbins, *Mol. Phys.* **78**:591 (1993).
20. K. Meier, A. Laesecke, and S. Kabelac, *Int. J. Thermophys.* **22**:161 (2001).
21. Y. Yang, T. A. Pakkanen, and R. L. Rowley, *Int. J. Thermophys.* **21**:703 (2000).